第33卷第1期
2014年2月

红外与毫米波学报
J. Infrared Millim. Waves

Vol. 33, No. 1
February, 2014

文章编号：1001－9014(2014)01－0023－08

DOI：10.3724/SP.J.1010.2014.00023

Extraordinary optical transmission in a periodically structured composite metal system

LI Ke, ZHENG Hou-Zhi*

(State Key Laboratory for Superlattices and Microstructures, Institute of Semiconductors, Chinese Academy of Sciences, Beijing 100083, China)

Abstract: Using full-vectorial, three dimensional, finite difference time domain (FDTD) simulator, greatly enhanced extraordinary optical transmission (EOT) is studied in a composite metal system, which is constructed by stacking a hexangular annular ring array over a hexangular hole array, perforated in a metallic film. In comparison with conventional periodic hole array, perforated in a single metal film, the composite metal system exhibits much stronger transmission amplitude and narrower band width. Such a novel behavior of EOT is well explained by the numerical results obtained from the distributions of electric field intensity, flowing maps of Poynting vectors and frequency dispersions. The results show that strongly excited surface plasmon polaritons (SPP) plays a dominant role in coupling light throughout the composite system.

Key words: subwavelength structures ; extraordinary optical transmission; surface plasmons ; finite difference time domain method

PACS: 78.66.Bz, 73.20.Mf, 42.25.Fx, 41.20.Jb

金属复合结构的反常透射增强效应的数值分析

李 轲, 郑厚植*

(中国科学院半导体研究所 超晶格国家重点实验室,北京 100083)

摘要：利用全矢量的三维时域有限差分法,分析了一种金属银复合结构的反常透射增强效应.该结构是在一层打有六角排列的圆孔阵列的金属银层的上方放置一层六角排列的银圆环阵列构成.与普通的单层银打孔阵列相比,该结构明显具有更高的透射峰值和更窄的透射带宽.系统分析了结构的场强分布、坡印廷矢量能流分布图、透射峰的频率色散关系,结果表明该复合结构激发的更强的独特的表面等离激元模式主导了整个透射过程.

关 键 词：亚波长结构;反常透射效应;表面等离激元;时域有限差分法

中图分类号：O431.1 **文献标识码**：A

Introduction

The discovery of the extraordinary optical transmission (EOT) of light through metal layers perforated periodically with sub-wavelength holes[1] provides a possibility for the efficient control of the spectrum and magnitude of light transmission, and makes them very promising for applications in novel photonic and optoelectronic devices[2]. Various pictures for EOT phenomena based on different physical models have been proposed. That, for examples, includes resonant tunneling transfer between surface plasmon polaritons (SPP) excited on both sides of a thin metal film (irrelevant to the structures perforated on it); penetration of the SPPs excited on one interface to the other interface through the localized electromagnetic field inside holes; the excitation of SPP Bloch waves in a two dimensional, metallic optical crystal and their subse-

Received date: 2012-10-25, **revised date**: 2013-07-13 **收稿日期**：2012-10-25, **修回日期**：2013-07-13

Foundation items: Supported by The National Basic Research Program of China(2011CB932901)

Biography: Li Ke(1984-), male, Yongxing, Hunan, Ph. D. Research area involves surface plasmons, optics.

* **Corresponding author**: E-mail: hzzheng@red.semi.ac.cn.

quent tunneling through it, etc[3-6]. While such a debate will still continue, more attention has been paid on the potential application of EOT. Among the other applications, EOT can be employed to engineer the spectral response of light as it passes through a metal film perforated with a periodic hole array. The important issue for using it as a spectrum filter is how to narrow spectrum width and to enhance intensity of transmitted light. Many means have been used for that purpose. Since there are mechanisms other than pure SPP-based one, like the excitation either of SPP Bloch waves on a periodic structure, or of various kinds of localized surface plasmons (LSP), to some extend, the variation in the parameters of a periodically perforated structure, such as film thickness, hole size and type etc. will change EOT both in its strength and spectrum. By coupling a Wood-Rayleigh anomaly (RWA) on one side of the film with a SPP Bloch wave on the opposite side, such a "RWA-SPP" effect can also bring about a strong variation in transmission amplitude[7,8]. However, the matching condition for RWA-SPP resonance requires that the dielectric constant of one surrounding medium beside the metal film should be adjustable.

In the present work, we use FDTD numerical simulator to study EOT phenomena in a composite metal system, which are constructed by stacking a hexangular annular ring array over a hexangular hole array perforated in a metallic film. EOT phenomena in such a composite metal system are substantially enhanced, giving rise to much large peak magnitude and a narrow band width in transmission spectra. Such a novel behavior of EOT is well explained by the numerical results, obtained from the distributions of electric field intensity, flowing maps of Poynting vectors and frequency dispersions.

1 Model system

Figure 1 schematically depicts our model system. The bottom layer is a thin Ag film of thickness h_1 perforated by hexangular array of holes, the diameter of which is denoted by D_3. The top layer is a hexangular array of Ag annular rings. The structures on the two layers have the same period P. The annular ring array is self-suspended either in air or placed on the top of dielectric medium layers on the bottom hole array. The two layers may be either separated by a spacer of d or stacked in close contact with each other ($d=0$). The thickness of annular rings is h_2, and their outer and inner diameters are labeled by D_1 and D_2, respectively. In all the cases we consider here, $D_1=D_3$. The (x, y, z) coordinate is defined as shown in Fig. 1. The light comes along z axis from the bottom and penetrates through our model system with its electric field (E_x, 0, 0) polarized in the x direction.

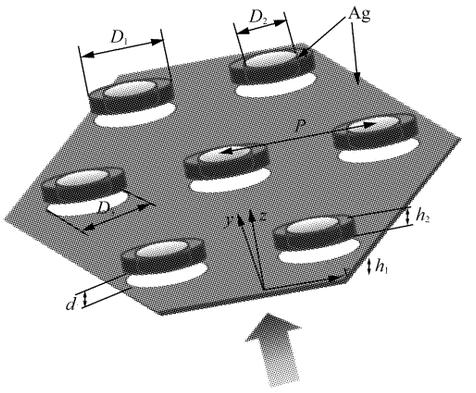

Fig. 1 Model system composed of a thin Ag film, perforated by hexangular array of holes, and a hexangular array of Ag annular rings stacked on the top. Geometric parameters: P, D_1, D_2, D_3, d, h_1, h_2 and x-y-z coordinate are defined as indicated

图1 研究的模型体系由一层打孔阵列的银膜和一层银圆环阵列相隔一定间隙叠加构成,圆孔阵列和圆环阵列均按六角格子排列. 几何参量: P, D_1, D_2, D_3, d, h_1, h_2 和 x-y-z 坐标系如图所示

2 Numerical simulations and discussions

2.1 Model used in numerical simulation

The methods for studying EOT phenomenon can generally be divided into two kinds. The first kind assigns a causative role played by various SPP modes in advance, including SPP mode, SPP Bloch mode, LSP mode etc. The advantage of SPP-based modes is that they can provide intuitive understanding of EOT phenomena. The second kind employs dynamic diffraction concepts by taking all the individual holes as elementary scatters and searches the model solutions of Maxwell's equations [9-10]. It turns out that the predictions obtained from SPP models capture quantitatively the main features of the data, for example, from the nu-

merical rigorous coupled-wave analysis (RCWA)[10]. As a result, we shall adopt full-vectorial three dimensional FDTD method (FDTD Solutions 7.5) to study the electromagnetic wave propagation through our composite metal system. The frequency dependent real and imaginary parts of Ag dielectric constant adopt the fitting curves given in FDTD Solutions 7.5 itself.

2.2 Normalized transmission of composite metallic system

In this section we first calculate the normalized transmission of periodically constructed, composite metallic system under different sets of parameters, and compare it with various kinds of single metal films perforated by different hole arrays. To make such comparison on an equal footing, EOT is characterized by the normalized transmission, defined as [11]

$T_{\text{norm}} = \dfrac{T}{S_{\text{hole}}/S_{\text{cell}}} = \dfrac{P_{\text{out}}}{P_{\text{in}}}\dfrac{S_{\text{cell}}}{S_{\text{holl}}}$, where T is the non-normalized transmission coefficient, T_{norm} the normalized transmission coefficient, S_{cell} the area of unit cell, and S_{hole} the hole's area in an unit cell. P_{in}, P_{out} are the input and output light intensities.

It is well known that the peak positions of the transmission at normal incidence in the EM field configuration shown in Fig. 1 can be approximately determined by applying the momentum-matching conditions to a two-dimensional hexangular array as given in a first approximation by[2]

$\lambda_{\max} = \dfrac{\sqrt{3}}{2} iP\sqrt{\dfrac{\varepsilon_m}{\varepsilon_m + 1}}$, where P is the period of the array, ε_m is the dielectric constants of the Ag metal and i is the scattering orders of the array along x direction. However, such a simple approach can not be employed in the composite metallic system discussed here. In order to make the various comparisons, the full-vectorial three dimensional FDTD method (FDTD Solutions 7.5) will be used throughout the present work.

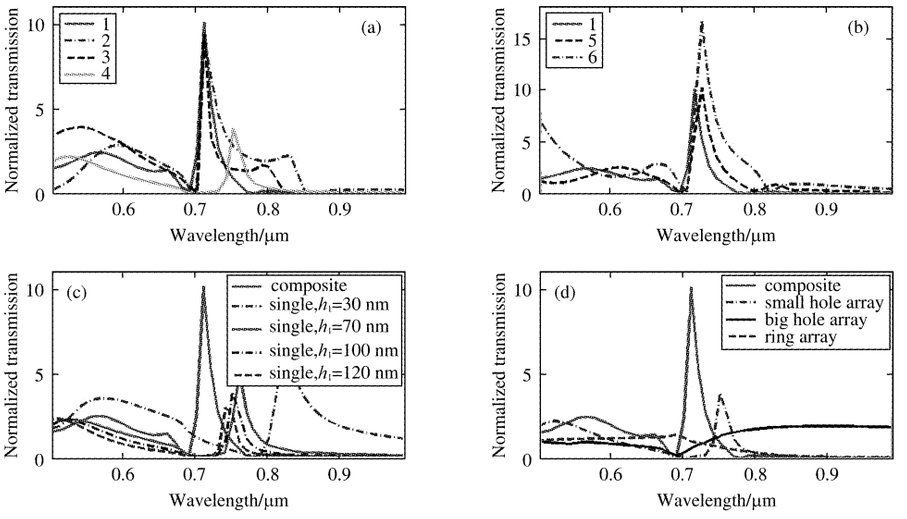

Fig. 2 (color online) (a) Nomalized EOT spectra of three composite Ag systems (1, 2, 3), as compared to a Ag film, perforated by periodic small holes (system 4). Their structure parameters are listed in Table 1. (b) A comparison of nomalized EOT spectra for three composite Ag systems (1,5,6) with the spacer being air, SiO_2 and SiN_x, respectively. Their structure parameters are listed also in Table 1 (c) Normalized EOT spectra of a Ag film, perforated by periodic holes, which have the same D_3 = 220 nm, P = 800 nm but different thicknesses of h_1 = 30, 70, 100, 120 nm. Nomalized EOT spectra of the composite Ag system 1 (see Table 1) is taken as the reference (d) Nomalized EOT spectrum of the composite Ag system 1, as compared to a small hole array (D_3 = 220 nm, P = 800 nm, h_1 = 100 nm), a big hole array (D_3 = 600 nm, P = 800 nm, h_1 = 30 nm) and an annular ring array (D_1 = 600 nm, D_2 = 220 nm, P = 800 nm, h_2 = 70 nm)

图 2 (a) 三个复合结构(见下表中 1,2,3 结构参量)和一个单层小孔阵列(见下表中 4 结构参量)的归一化透射曲线对比. (b) 三种不同复合结构(见下表中 1,5,6)的归一化透射曲线对比,它们的间隙填充介质分别是空气、SiO_2 和 SiN_x. (c) 复合结构 1 与四种不同厚度的单层银孔阵列的归一化透射比较,四种厚度分别是 30、70、100、120 nm,四种情况的圆孔直径都是 220 nm,阵列周期 800 nm. (d)复合结构 1 与单层小孔阵列(D_3 = 220 nm, P = 800 nm, h_1 = 100 nm)、单层大孔阵列(D_3 = 600 nm, P = 800 nm, h_1 = 30 nm)、单层圆环阵列(D_1 = 600 nm, D_2 = 220 nm, P = 800 nm, h_2 = 70 nm)的归一化透射曲线对比

Figure 2(a) plots the spectra of T_{norm} for three different, periodically constructed, composite Ag systems (1,2,3), while the T_{norm} spectrum for a hole array perforated on an Ag film(4) is taken as the reference. Their detailed parameters are listed in Table 1. For three composite Ag systems(1,2,3), no matter how D_1 and D_3 vary (always $D_1 = D_3$), the maximum of normalized transmission appears at the same wavelength of 0.714 μm as long as D_2 remains unchanged, and so does the Wood-Rayleigh minimum (approximately at 0.7 μm)[7,8]. Obviously, the composite Ag structure (1) represents the optimal case, where the transmission peak is the sharpest and of the highest magnitude with the background being lowest on both sides of the peak. In contrast, the single Ag layer (4) of the same D_2 shows a transmission peak at a different wavelength of 0.755 μm. Its peak magnitude is smaller than that of the composite Ag structure by a factor of 2.5.

Table 1 Structure parameters for five composite-and one single-Ag film systems

表1 五个复合结构和一个单层银膜的结构参量

Parameter	1	2	3	4	5	6
D_1(nm)	600	680	480	—	600	600
D_2(nm)	220	220	220	—	220	160
D_3(nm)	600	600	480	220	600	600
d(nm)/medium	20/air	0	20/air	—	20/SiO_2	20/Si_3N_4
h_1(nm)	30	30	30	100	30	30
h_2(nm)	70	70	70	—	55	40
P(nm)	800	800	800	800	800	800

For the practical use, the top array of the periodic annular rings can not be just suspended in air above the bottom hole array. We examine how the EOT changes if the spacer region between two arrays is filled by dielectric media like SiO_2 ($\varepsilon_d \sim 1.5$) or SiN_x ($\varepsilon_d \sim 2.0$). Fig. 2b compares three normalized transmission spectra for structures 1, 5, 6 (see Table 1) with structure 5, 6 having a 20 nm-thick SiO_2 layer and a 20 nm-thick SiN_x layer in the spacer region, respectively. As can be seen, the main EOT peak in the composite layer system 5 (SiO_2) keeps approximately the same as in the composite layer system 1, while the EOT peak position shifts slightly. The EOT peak amplitude of the composite layer system 6 (SiN_x) is strongly enhanced as compared with the composite layer system 1. After adjusting the geometric parameters of systems 5 and 6 properly, the EOT spectra in three systems become very similar. Therefore, the composite layer system proposed in the present work can actually be fabricated, making them promising in engineering the light spectrum through it.

A further comparison between composite and singal Ag layer systems is given in Fig. 2(c). The composite Ag layer system takes a fixed set of parameters: D_1 = 600 nm, D_2 = 220 nm, D_3 = 600 nm, P = 800 nm, h_1 = 30 nm, h_2 = 70 nm. The single Ag layer system has the parameters: D_3 = 220 nm, P = 800 nm and different thichnesses of h_1 = 30、70、100、120 nm, respectively. As shown in Fig. 2(c), the transmission peak of the singal Ag layer system shifts continuously from 0.827 μm to 0.745 μm with increasing the film thickness. Meanwhile, the peak becomes narrower, and the backgound on both sides of the peak is also suppressed at the same time. Unfortunately, the peak magnitude become substantially small as well. If the transmission peak moves to the same wavelength (0.714 μm) as that in the composite layer system, the peak magnitude will become further smaller. Therefore, the advantage of the composite Ag layer system over the single one is very obvious.

Figure 2(d) compares the transmission spectrum of the composite Ag layer system to the spectra of the single Ag layer system perforated by small or big holes, and to the spectrum of the hexangular array of Ag annular rings as well. Their parameters are described in the figure. Except that the spectrum of the small-hole-perforated film exhibits the same behavior as in Fig. 2(a), (c), the spectrum of the big-hole-perforated film only shows the Wood-Rayleigh minimum without any peak feature. The array of annular rings seems to exhibit a weak bump at the wavelength of Wood-Rayleigh abnormally due to coherent diffraction by the annular rings. Therefore, the unique feature displayed in the composite Ag layer system results from the special structure combination.

2.3 Distribution of the total electric field strength in periodically structured, composite-and single-Ag layer systems

To understand the huge enhancement of EOT in

the periodically structured, composite Ag layer system, we numerically calculate the distribution of the total electric field strength, $|E|^2 = |E_x|^2 + |E_z|^2$, and compare it with that in single Ag layer systems perforated periodically by holes of different sizes.

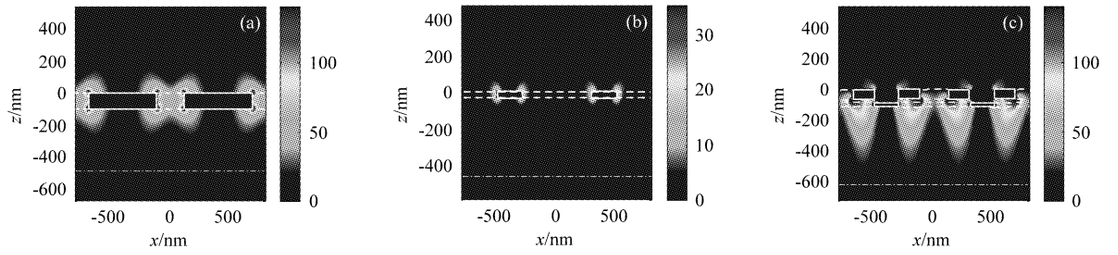

Fig. 3 (color online) $|E|^2$ distribution in x-z plane, calculated (a) at $\lambda = 755$ nm for small hole array ($D_3 = 220$ nm, $P = 800$ nm, $h_1 = 100$ nm) (b) at $\lambda = 714$ nm for big hole array ($D_3 = 600$ nm, $P = 800$ nm, $h_1 = 30$ nm) (c) at $\lambda = 714$ nm for the composite Ag system 1 in Table 1. Their light sources are located at $z = -480$ nm, -460 nm and -630 nm, respectively, as indicated by dashed horizontal lines

图 3　x-z 平面内的 $|E|^2$ 分布(a) 波长 755 nm,小圆孔阵列($D_3 = 220$ nm, $P = 800$ nm, $h_1 = 100$ nm)(b) 波长 714 nm, 大圆孔阵列($D_3 = 600$ nm, $P = 800$ nm, $h_1 = 30$ nm)(c) 波长 714 nm,复合结构 1(见表 1). 图中入射光源位置分别位于 $z = -480$ nm, -460 nm 和 -630 nm,如图中下方白色虚线位置

Figure 3(a) shows $|E|^2$ distribution when the light, emitted from $z = -480$ nm, penetrates a 100 nm-thick Ag film perforated by hole array of a diameter of $D_3 = 220$ nm and a period of $P = 800$ nm. Since the area ratio of holes is small, SPP mode is excited on the incoming surface of the Ag film because that the interaction of SPP with small surface structures is rather weak. The additional coupling through the holes is fulfilled by LSP modes. However, the similar spatial distribution of $|E|^2$ also appear on the outgoing surface of the Ag film. For the large hole array ($D_3 = 600$ nm, $P = 800$ nm) perforated in a 30 nm-thick Ag film, $|E|^2$ distribution is numerically calculated as the light source is located at $z = -460$ nm. No SPP excitation is discernible as evidenced from Fig. 3b. This is because the total area of the holes is larger than the area of the remaining metal surface. For such a perforated metallic film, surface plasmon polaritons cannot be sustained. In this case, LSP in a single hole and their interaction between different holes in such an Ag film dominants the enhanced transmission. However, one should know that the strength of $|E|^2$ in Fig. 3(b) is much weaker than that in Fig. 3a by noticing that the color scales used in two figures differ by a factor of 4.

In Fig. 3(c), the $|E|^2$ distribution in the periodically structured, composite Ag system is also numerically calculated as the light shines from $z = -630$ nm. It exhibits very different behavior from that in both the small hole and large hole arrays, perforated in 100 nm- and 30 nm-thick Ag films, respectively. In contrast to intuitive unders tanding that SPP is more easy excited on a smooth metallic surface, the very intensive SPP is indeed excited on the rugged incoming surface, and confined inside the big holes. Meanwhile, the SPP on the outgoing surface appears similar to that in Fig. 3(a). This intrigue feature of the $|E|^2$ distribution in Fig. 3(c) explains the huge enhancement of the transmission coefficient shown in Fig. 2.

2.4 Flowing maps of Poynting vectors in periodically structured, composite-and single-Ag layer systems

To illustrate intuitively how the light energy flows as the enhanced EOT goes on in the periodically structured, composite Ag system, both the intensity (depicted by the color scale) and flowing direction (indicated by arrows) of Poynting vectors in z-x plane were calculated in comparison with that in the single Ag layer periodically perforated by holes.

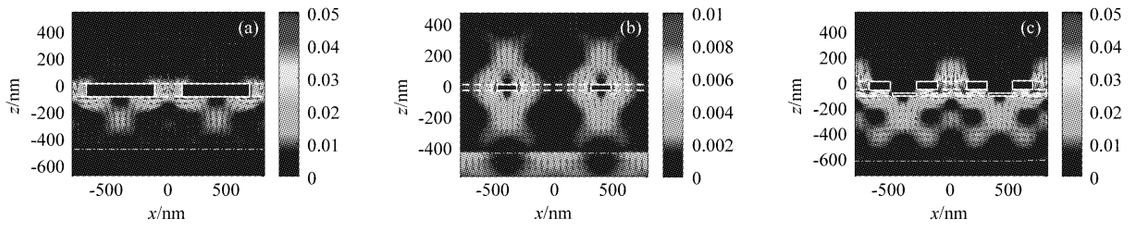

Fig. 4 (color online) Flowing maps in x-z plane of both the intensity, as depicted by the color scale, and flowing direction, as indicated by arrows, of Poynting vectors, calculated (a) at $\lambda = 755$ nm for a small hole array ($D_3 = 220$ nm, $P = 800$ nm, $h_1 = 100$ nm) (b) at $\lambda = 714$ nm for a big hole array ($D_3 = 600$ nm, $P = 800$ nm, $h_1 = 30$ nm) (c) at $\lambda = 714$ nm for the composite system 1 (see Table 1). Location of incident light source are the same as in Fig. 3

图4 x-z 平面内能流图,彩色亮度表示能流大小,小箭头表示能流方向(a) 波长 755 nm,小圆孔阵列($D_3 = 220$ nm, $P = 800$ nm, $h_1 = 100$ nm)(b) 波长 714 nm,大圆孔阵列($D_3 = 600$ nm, $P = 800$ nm, $h_1 = 30$ nm)(c) 波长 714 nm,复合结构 1 (见表 1). 下方白色虚线表示入射光源位置,同上面图 3

Figure 4(a) and (b) are the numerical simulation results for the single Ag films perforated by small hole and big hole arrays with the light sources located at $z = -480$ nm and $z = -460$ nm, respectively. Their common feature is the appearance of vortex pattern on both incoming and outgoing sides of the Ag film, reflecting the coherent interference in the systems. These vortexes also prevent incident light right underneath holes from penetrating through them directly. By a close look, however, one finds that the Poynting vectors flow quite differently in these two systems. In Fig. 4(a), the incoming Poynting vectors impinge vertically on the central parts between adjacent holes, then turns to parallel to the incoming surface as a result of its conversion into SPP modes. Then, the Poynting vectors are coupled out of holes. In this case, the SPP mode is indeed excited, and plays an important role in EOT phenomena. However, as seen from Fig. 4(b), the incoming Poynting vectors directly enter the big holes through their coupling with LSP modes. As shown in Fig. 4(c), the flowing map of the Poynting vectors in the periodically structured, composite Ag system is quite similar to that in Fig. 4(a). However, the Poynting vectors, related to the excited SPP, are mainly localized inside the big holes, and are of much higher intensity than that in Fig. 4(a). As a result, the intensity of the energy flowing, coupling out of it, is much stronger than that in Fig. 4(a) as well.

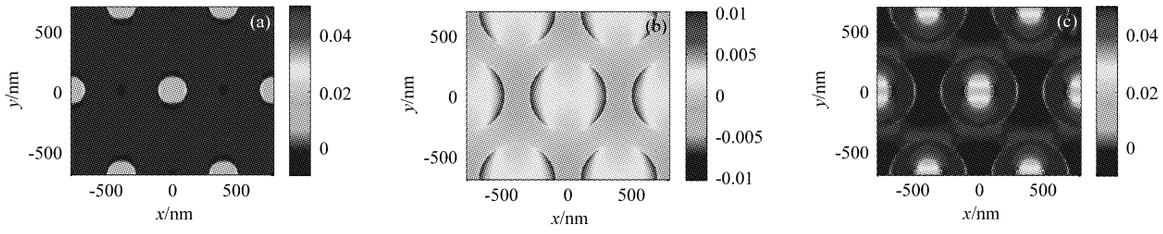

Fig. 5 (color online) The intensity of z component of Poynting vectors in x-y plane on outgoing surface, calculated (a) at $\lambda = 755$ nm for a small hole array ($D_3 = 220$ nm, $P = 800$ nm, $h_1 = 100$ nm) (b) at $\lambda = 714$ nm for a big hole array ($D_3 = 600$ nm, $P = 800$ nm, $h_1 = 30$ nm) (c) at $\lambda = 714$ nm for the composite system 1 (in Table 1)

图5 出射面位置 x-y 平面内坡印廷矢量的 z 方向分量分布的几种情况(a) 波长 755 nm,小圆孔阵列($D_3 = 220$ nm, $P = 800$ nm, $h_1 = 100$ nm)(b) 波长 714 nm,大圆孔阵列($D_3 = 600$ nm, $P = 800$ nm, $h_1 = 30$ nm)(c) 波长 714 nm,复合结构 1(见表 1)

This can also be seen from Fig. 5(a), (b), (c), where the intensity distribution of the z component of Poynting vectors inside the small holes in x-y plane, measured at the outgoing surface, is highest in the periodically structured composite Ag system. The intensity distributions of the energy flowing in Fig. 4(a) and 4(c) are quite similar, but the latter is much more intensive than the former. Meanwhile, the

big hole exhibits an intensity distribution characteristic of two-lobe structure as shown in Fig. 4(b).

2.5 EOT reversibility in the periodically structured, composite Ag layer system

Generally speaking, an asymmetric system, like the periodically structured composite Ag system discussed here, would not give rise to a symmetric EOT phenomenon as the structure turns upside down. Figure 6 compares EOT spectra for the normal and reversed composite Ag systems.

The spectrum position, magnitude and bandwidth of the transmission peak in the reversed composite Ag system remains nearly the same as that in the normal one. The difference between them appears mainly on the short wavelength side of the EOT peak.

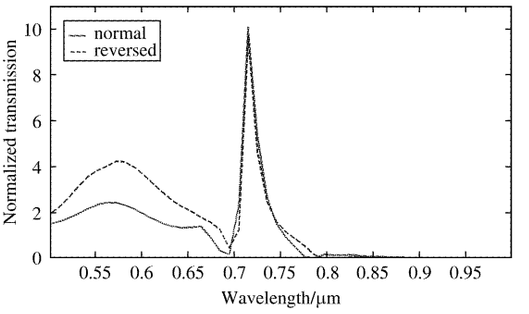

Fig. 6 (color online) A comparison of EOT spectra between two cases: one is for big hole array to face incident light(normal), the other is for annular ring array to face incident light(reversed)

图 6　正反两种放置的透射对比,红色实线代表圆孔面向入射光的正入射,蓝色虚线代表圆环面向入射光的反向放置

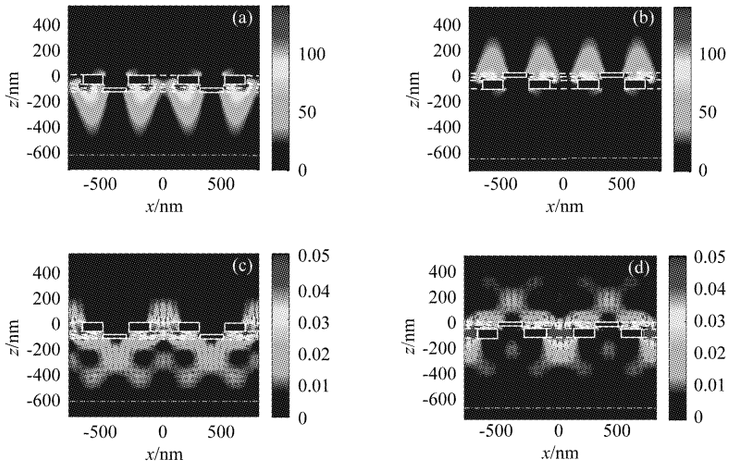

Fig. 7 (color online) $|E|^2$ distribution in x-z plane calculated at $\lambda = 714$ nm (a) for the normal case with big hole array facing incident light (b) for the reversed case with annular ring array facing incident light. Flowing maps in x-z plane of both the intensity (as depicted by the color scale) and flowing direction (as indicated by arrows) of Poynting vectors were calculated at $\lambda = 714$ nm (c) for the normal case (d) for the reversed case. Light source is located at $z = -630$ nm

图 7　x-z 平面内峰值波长 714 nm 的 $|E|^2$ 分布(a) 大圆孔面向入射光的正入射情况(b) 圆环阵列面向入射光的反置情况. x-z 平面内峰值波长 714 nm 的能流图,彩色亮度代表能流的大小,箭头显示能流方向(c) 正入射情况(d) 反置情况. 光源位置在 $z = -630$ nm

Figure 7 shows the $|E|^2$ distribution and flowing map of the Poynting vectors for both the normal and reversed composite Ag systems. One can clearly find their similarities. Especially, their flowing maps of the Poynting vectors almost exhibit inversion symmetry. Such EOT reversibility is somewhat unexpected in an asymmetric composite Ag layer system.

2.6 Dispersion of EOT in the periodically structured, composite Ag layer system

It is well established that a periodic hole array perforated on Ag film may generate a complex band structure of SPP, and makes it a SPP Bloch wave. Coupling of incident light to the silver/air SPP Bloch mode via different order scattering can make some

branch of SPP frequency dispersion curves to show up inside the light cone[2]. To examine if the frequency dispersion curves of SPP Bloch mode hold also for the present composite Ag system, the numerically calculated transmission in Fig. 8 is expressed in a color-scale as functions of both the incident wavelength and the angle of the incident plane wave. The corresponding frequency dispersion curves in the single hole array are also shown in the figure for comparison.

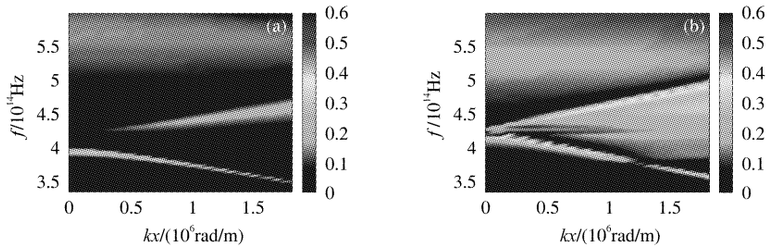

Fig. 8 (color online) Frequency dispersions of EOT are expressed in a color-scale with the variations of both the incident wavelength and the angle of the incident wave. (a) Frequency dispersion for small hole array (D_3 = 220 nm, P = 800 nm, h_1 = 100 nm) (b) frequency dispersion for the composite system 1 (see table 1)
图 8 通过改变入射角获得的透射峰频率的色散曲线彩图. (a) 单层小圆孔阵列的情况(D_3 = 220 nm, P = 800 nm, h_1 = 100 nm) (b) 复合结构 1 的情况(见表 1)

Figure 8 (a) displays the frequency dispersion curves calculated for the periodic hole array (D_3 = 220 nm, P = 800 nm, h = 100 nm). The up and low braches can be assigned to (+1, 0) and (−1, 0) modes[12]. Interestingly, the composite Ag system also shows similar frequency dispersion curves for (+1, 0) and (−1, 0) modes as shown in Fig. 8(b). Therefore, SPP Bloch wave indeed takes place in the composite Ag system. That is somewhat unexpected in composite metal layers used here.

3 Conclusions

The EOT phenomenon has been studied by FDTD numerical simulator in a composite metal system, which are constructed by stacking a hexangular ring array right over a hexangular hole array perforated on a Ag film. The EOT spectrum of this system shows a strongly enhanced, narrow transmission peak as compared with that in the hole-perforated single Ag film. Both the calculated $|E|^2$ distributions and flowing maps of Poynting vector illustrate that the strongly excited SPP plays a dominant role in coupling more light out of the composite Ag system. Interestingly, the ragged incoming surface does not seem to destroy the SPP excitation. On opposite, SPP is excited much strong. Moreover, it is somewhat intrigue that EOT in our asymmetric composite metallic system has approximately the property of the reversibility as the light shines from the two opposite sides. It was also found that the frequency dispersion of the composite Ag system has two branches, labeled by (−1, 0) and (1, 0) respectively, inside the light cone in the spectrum range from 500 nm to 1 000 nm, which are similar to that in the hole-perforated single Ag film. The appearance of the complex SPP band structure demonstrates that the SPP Bloch wave is indeed excited in our composite system. Because the enhanced EOT does not strongly depend on which medium is used in the spacer between two layers, our composite metallic system may find its potential application in engineering light spectrum and being used as a color filter.

REFERENCES

[1] Ebbesen T. W, Lezec H. J, Ghaemi H. F, *et al*. Extraordinary optical transmission through subwavelength hole arrays[J]. *Nature*, 1998, **391**(6668): 667−669.
[2] Genet C, Ebbesen T. W, Light in tiny holes[J]. *NATURE*, 2007, **445**: 39−46.
[3] Martin-Moreno L, García-Vidal F J, Lezec H. J, *et al*. Theory of Extraordinary Optical Transmission through Subwavelength Hole Arrays[J]. *Phys. Rev. Lett*. 2001, **86**: 1114−1117.
[4] Tan W C, Preist T W, Sambles R J, Resonant tunneling of light through thin metal films via strongly localized surface

(下转第 49 页)

2D-PC with respect to the lattice constant and column diagonal in the area of 12×12 μm^2 has also been carried out. According to the statistical study, the nonuniform of the lattice constant and column diagonal with period of 1 μm is 2.9% and 3.6%, while the nonuniform of the lattice constant and column diagonal with period of 2 μm is 3.4% and 4.9%, respectively.

3 Conclusions

In conclusion, column shape 2D-PC on InP substrate have been fabricated by using holographic lithography technique. Adopting double development process, big-dot-type periodic structures have been generated on positive photoresist directly with easily controlled exposure dose and developing time. Si_3N_4 hard mask is chosen to transfer the dot-type periodic structures into the substrate due to its high selectivity in dry etching process. The period of the structures can be easily controlled by adjusting the angle of the two incident beams. 2D-PC samples in an area of larger than 2×2 cm^2 with good uniformity and reproducibilityhave been fabricated successfully, validated the feasibility of this unique process in the applications of various devices.

REFERENCES

[1] Chow E, Lin S Y, Jonhson S G, *et al*. Three-dimensional control of light in a two-dimensional photonic crystal slab [J]. *Nature*, 2000, **407**(26): 983 - 986.

[2] Akahane Y, Asano T, Song B S, *et al*. High-Q photonic nanocavity in a two dimensional photonic crystal[J]. *Nature*, 2003, **425**(30): 944 - 947.

[3] Painter O, Lee R K, Scherer A, *et al*. Two-Dimensional Photonic Band-Gap Defect Mode Laser[J]. *Science*, 1999, **284**(11): 1819 - 1821.

[4] Lin J H, Huang Y C, Lai N D, *et al*. Optical modulation of guided mode resonance in the waveguide grating structure incorporated with azo-doped-polycladding layer[J]. *Optics Express*, 2012, **20**(1): 377 - 384.

[5] Hofmann H, Scherer H, Deubert S, *et al*. Spectral and spatial single mode emission from a photonic crystal distributed feedback laser[J]. *Applied Physics Letters*, 2007, **90**(12): 121135.

[6] Bai Y, Darvish S R, Slivken S, *et al*. Electrically pumped photonic crystal distributed feedback quantum cascade lasers[J]. *Applied Physics Letters*, 2007, **91**(14): 141123.

[7] Sugimoto Y, Ikeda N, Carlsson N, *et al*. Fabrication and characterization of different types of two-dimensional AlGaAs photonic crystal slabs[J]. *Journal of Applied Physics*, 2001, **91**(3): 922 - 929.

[8] Lu C, Lipson R H, Interference lithography: a powerful tool for fabricating periodic structures[J]. *Laser Photonics Reviews*, 2010, **4**(4): 568 - 580.

[9] Xu G Y, Li A Z, Li Y Y, *et al*. Low threshold current density distributed feedback quantum cascade lasers with deep top gratings[J]. *Applied Physics Letters*, 2006, **89**(16): 161102.

[10] Li Y Y, Li A Z, Wei L, *et al*. High-Temperature Operation of 8.5 μm Distributed Feedback Quantum Cascade Lasers[J]. *Chinese Physics Letters*, 2009, **26**(8): 087804.

[11] Lai N D, Liang W P, Lin J H, *et al*. Fabrication of two- and three-dimensional periodic structures by multi-exposure of two-beam interference technique[J]. *Optical Express*, 2005, **13**(23): 9605 - 9611.

[12] Zhong Y C, Zhou J Y, Wong K S. Two-photon fabrication of photonic crystals by single-beam laser holographic lithography[J]. *Journal of Applied Physics*, 2010, **107**(7): 074311.

[13] Campbell M, Sharp D N, Harrison M T, *et al*. Fabrication of Photonic crystals for the visible spectrum by holographic lithography[J]. *Nature*, 2000, **404**(2): 53 - 56.

[14] Lai N D, Liang W P, Lin J H, *et al*. Rapid fabrication of large-area periodic structures containing well-defined defects by combining holography and mask techniques[J]. *Optical Express*, 2005, **13**(14): 5331 - 5337.

[15] Xie Q, Hong M H, Chen G X, *et al*. Fabrication of nanostructures with laser interference lithography[J]. *Journal of Alloys and Compdounds*, 2008, **449**(1): 261 - 264.

(上接 30 页)

plasmons[J]. *Phys. Rev. B*. 2000, **62**: 11134 - 11138.

[5] Krishnan A, Thio T, Kim T J, *et al*. Evanescently coupled resonance in surface plasmon enhanced transmission[J]. *Opt. Commun*. 2001, **200**: 1 - 7.

[6] Gerard D, Salomon L, Fornel F de , *et al*. Ridge-enhanced optical transmission through a continuous metal film[J]. *Phys. Rev. B*, 2004, **69**: 113405 - 1 - 13405 - 4.

[7] Jeffrey M. McMahon, Joel Henzie, Teri W Odom, *et al*. Tailoring the sensing capabilities of nanohole arrays in gold films with Rayleigh anomaly-surface plasmon polaritons[J]. *Optics Express*, 2007, **15**: 18119 - 18129.

[8] Gao H, McMahon J M, Lee M H, *et al*. Rayleigh anomaly-surface plasmon polariton resonances in palladium and gold subwavelength hole arrays[J]. *Optics Express*, 2009, **17**: 2334 - 2340.

[9] Treacy M M J, Dynamical diffraction explanation of the anomalous transmission of light through metallic gratings[J]. *Phys. Rev. B* 2002, **66**: 195105 - 1 - 195105 - 11.

[10] Haitao Liu , Philippe Lalanne. Microscopic theory of the extraordinary optical Transmission [J]. *Nature*, 2008, **452**: 728 - 731.

[11] Zhichao Ruan , Min Qiu. Enhanced transmission through periodic arrays of subwavelength holes: the role of localized waveguide resonances [J]. *Phys Rev. Lett*. 2006, **96**: 233901 - 1 - 233901 - 4.

[12] Barnes W L, Murray W A, Dintinger J, *et al*. Surface plasmon polaritons and their role in the enhanced transmission of light through periodic Arrays of subwavelength holes in a metal film[J]. *Phys Rev. Lett*. 2004, **92**: 107401 - 1 -107401 - 4.